Published online 16 July 2008

Nucleic Acids Research, 2008, Vol. 36, No. 14 ***4719–4726***
doi:10.1093/nar/gkn440

Phosphorylation of the carboxy-terminal domain of histone H1: effects on secondary structure and DNA condensation

Alicia Roque[1], Inma Ponte[1], José Luis R. Arrondo[2] and Pedro Suau[1,*]

[1]Departamento de Bioquímica y Biología Molecular, Facultad de Biociencias, Universidad Autónoma de Barcelona, 08193 Bellaterra, Barcelona, Spain and [2]Departamento de Bioquímica, Universidad del País Vasco, Apartado 644, E-48080, Bilbao, Spain

Received May 15, 2008; Revised and Accepted June 26, 2008

ABSTRACT

Linker histone H1 plays an important role in chromatin folding. Phosphorylation by cyclin-dependent kinases is the main post-translational modification of histone H1. We studied the effects of phosphorylation on the secondary structure of the DNA-bound H1 carboxy-terminal domain (CTD), which contains most of the phosphorylation sites of the molecule. The effects of phosphorylation on the secondary structure of the DNA-bound CTD were site-specific and depended on the number of phosphate groups. Full phosphorylation significantly increased the proportion of β-structure and decreased that of α-helix. Partial phosphorylation increased the amount of undefined structure and decreased that of α-helix without a significant increase in β-structure. Phosphorylation had a moderate effect on the affinity of the CTD for the DNA, which was proportional to the number of phosphate groups. Partial phosphorylation drastically reduced the aggregation of DNA fragments by the CTD, but full phosphorylation restored to a large extent the aggregation capacity of the unphosphorylated domain. These results support the involvement of H1 hyperphosphorylation in metaphase chromatin condensation and of H1 partial phosphorylation in interphase chromatin relaxation. More generally, our results suggest that the effects of phosphorylation are mediated by specific structural changes and are not simply a consequence of the net charge.

INTRODUCTION

H1 linker histones are involved in chromatin structure and gene regulation (1). Histone H1 contains three distinct domains: a short amino-terminal domain (20–35 amino acids), a central globular domain (~70 amino acids) and a long carboxy-terminal domain (CTD) (~100 amino acids) (2). Several studies indicate that the ability of linker histones to stabilize chromatin folding resides in the CTD of the molecule (3). The CTD displays a high degree of conformational flexibility. In aqueous solution, the CTD is dominated by the random coil and turn-like conformations in rapid equilibrium with the unfolded state, but when it interacts with DNA it folds cooperatively. The DNA-bound structure is extremely stable and includes α-helix, β-sheet, turns and open loops (flexible regions) (4). The H1 CTD thus appears to belong to the so-called intrinsically disordered proteins undergoing coupled binding and folding (5–7). In addition, in the presence of macromolecular crowding agents the unbound CTD acquires the properties of a molten globule with native-like secondary structure and compaction (8).

The phenotypic roles of histone H1 may be determined by complementary and overlapping effects of stoichiometry, subtype composition and post-translational modifications. Phosphorylation of the consensus sequences of cyclin-dependent kinases (CDKs), (S/T)-P-X-(K/R), is the main post-translational modification affecting histone H1 (9). In mammalian subtypes these sequences are localized mostly in the CTD. The maximum number of phosphate groups often corresponds to the number of CDK sites in the molecule. Histone H1 is phosphorylated in a cell cycle-dependent manner. The levels of phosphorylation are lowest in G1 and rise during S and G2 (10,11). During interphase, H1 subtypes are present as a mixture of unphosphorylated and low-phosphorylated species with a proportion of 35–75% of unphosphorylated forms, according to the particular subtype and cell line and the moment of the cell cycle. The highest number of phosphorylated sites is found in mitosis, when chromatin is maximally condensed. Phosphorylation of H1 variants may occur site-specifically during the phases of the cell cycle (12).

It is not clear how H1 phosphorylation affects chromatin condensation during interphase and mitosis. A number

*To whom correspondence should be addressed. Tel: +34 93 5811391; Fax: +34 93 5811264; Email: pere.suau@uab.es

of studies indicate that interphase phosphorylation is involved in chromatin relaxation (13–15); however, in metaphase chromosomes, H1 is hyperphosphorylated, and it has been shown that H1 hyperphosphorylation is required to maintain metaphase chromosomes in their condensed state (16).

Here we report the effects of partial and full phosphorylation on the secondary structure of the CTD of histone H1 using IR spectroscopy. We have also estimated the relative affinities for the DNA and the DNA condensing capacity of the different phosphorylated species of the CTD. The results, showing site-specific effects depending on the number and position of phosphate groups may contribute to reconcile the roles of H1 phosphorylation in interphase and mitosis.

MATERIALS AND METHODS

Cloning, expression and purification of the CTD

The CTD of histones H1° and H1e were obtained from recombinant *Escherichia coli* (M15) as described previously (4). The sequence encoding the CTD of histone H1e was amplified from mouse genomic DNA by PCR. The primers used for the amplification reaction were 5′AAACTC CATATGAAGGCGGCTTCCGGTGAG3′ and 5′GAA CTCGAGCTTTTTCTTGGCTGCTTT3′. The amplification products were cloned in the pET21 vector (Novagen; Darmstadt, Germany) using the NdeI and XhoI restriction sites to yield the expression vector pCTH1e. The recombinant protein was expressed in *Escherichia coli* BL21 and purified as described for the CTD of histone H1° (CH1°).

Construction of mutants of the CDK2 sites

The mutant clones for the CDK2 phosphorylation sites of the CH1° were obtained by PCR using the QuickChange Site-directed Mutagenesis Kit (Strategene; Amsterdam, Netherlands) following the manufacturer's instructions. The primers used for each phosphorylation site were mutated so that the threonine residue was changed to alanine. For threonine at position 118 the primers were 5′TCAA GAAAGTGGCAGCTCCAAAGAAGGCA3′ and 5′TG CCTTCTTTGGAGCTGCCACTTTCTTGA3′. For position T140 the primers were 5′AGAAACCCAAAGCCGC CCCTGTCAAGAAG3′ and 5′CTTCTTGACAGGGG CGGCTTTGGGTTTGGGTTTCT3′. For position T152 the primers were 5′GCTGCCGCGCCCAAGAAAGCAA AAAGCC3′ and 5′GGCTTTTTGGCTTTCTTGGGCG CGGCAGC3′. Double and triple mutants were obtained in successive rounds of PCR. The introduction of the correct mutation was evaluated by DNA sequencing of the recombinant clones. The recombinant plasmids were named according to the position mutated in each case. Clones were expressed and purified as described for the wild-type CTD.

In vitro phosphorylation assay

The CTD of histone H1 subtypes were phosphorylated *in vitro* with CDK2-cyclin A kinase (New England Biolabs; Ipswich, MA, USA). Phosphorylation reactions were carried out in 50 mM Tris.HCl, 10 mM $MgCl_2$, 1 mM EGTA, 20mM dithiotreitol, pH 7.5, plus 200 μM ATP and 1 U of CDK2-cyclin A per 5 μg of CTD. The mixture was incubated at 30°C for 1 h and the reaction buffer was eliminated by gel filtration on a HiTrap desalting column (GE Healthcare; München, Germany). The extent of phosphorylation was evaluated by MALDI-TOF mass spectrometry.

IR spectroscopy

The CTD of histone H1 were measured at 50mg/ml in 10 mM HEPES, pH 7.0 plus 140 mM NaCl. DNA–protein complexes contained the appropriate amount of DNA for each protein/DNA ratio (w/w): Measurements were performed on a Nicolet Magna II 5770 spectrometer equipped with a MCT detector, using a demountable liquid cell with calcium fluorine windows and 50 μm spacers for D_2O medium and 6 μm spacers for H_2O medium measurements. Typically, 1000 scans for each background and sample were collected and the spectra were obtained with a nominal resolution of 2 cm^{-1}, at 22°C. The protein concentration for the D_2O measurements was 5 mg/ml, while for the H_2O measurements it was 20 mg/ml. The spectra of the complexes were recorded both in H_2O and D_2O to facilitate the assignment of the amide I components (4). Data treatment and band decomposition were as previously described (17). The DNA contribution to the spectra of the complexes with the C-terminus was subtracted using a DNA sample of the same concentration; the DNA spectrum was weighted so as to cancel the symmetric component of the phosphate vibration at 1087 cm^{-1} in the difference spectra as described in (18).

Affinity measurements

The apparent relative affinities of the unphosphorylated and the different phosphorylated species of CH1° were estimated in competition experiments as previously described (19). The different forms of CH1° were made to compete with an approximately equal amount of the CTD of histone H1t (CH1t). A total of 3.0 μg of CTD was mixed with 0.5 μg of DNA in a final volume of 25 μl in 0.14 M NaCl, 0.01 M phosphate buffer, pH 7.0, 5% glycerol. The complexes were recovered by centrifugation at 14 000 *g* for 10 min. The protein composition of the complexes and of the free protein left in the supernatant was analyzed by SDS-PAGE and visualized by staining with Amido Black. The relative affinities were obtained with the expression:

$$k_{\mathrm{DNA}}^{i/j} = ([i\mathrm{DNA}][j]_{\mathrm{free}})/([jDNA][i]_{\mathrm{free}})$$

where the concentration of complexes, [*i*DNA] and [*j*DNA], was obtained from the band intensities in the pellets and the concentration of free protein, $[i]_{\mathrm{free}}$ and $[j]_{\mathrm{free}}$, from the band intensities of the supernatants.

Band shift gel electrophoresis

Complexes were formed in 0.14 M NaCl, 10 mM phosphate buffer, pH 7.0 and incubated at room temperature for 30 min before separation on 1% agarose gels. The

electrophoresis buffer was 36 mM Tris, 30 mM NaH_2PO_4, 1 mM EDTA, pH 7.7 (20). Gels were stained with ethidium bromide. The dsDNA fragment of 50 bp used in complex formation was obtained by annealing the oligonucleotide 5′CTATGATATATAGATAGTTAATGTAA TATGATATAGATATAGGGATCC3′ with its complementary sequence. The dsDNA fragment of 108 bp was obtained from pUC19 by PCR using the primers 5′GC GGTTAGCTCCTTCGGTCCTC3′ and 5′GGATGGC ATGACAGTAAGAGAA3′.

RESULTS

Conformational changes associated to full phosphorylation of the DNA-bound CTD of histone H1

The apparently conflicting roles of H1 phosphorylation suggest the existence of specific effects that depend on the number and position of phosphate groups. This led us to examine the secondary structure of the different phosphorylated forms of the DNA-bound CTD using IR spectroscopy. The CH1° contains three CDK sites. Phosphorylation of CH1° at all three sites brought about a large structural rearrangement characterized by a decrease in the proportion of α-helix and an increase in that of β-sheet (Figure 1; Table 1). The extent of the structural change appeared to be dependent on the protein to DNA ratio (***r***, w/w). At ***r*** = 0.25 or lower the α-helix decreased from 24% in the unphosphorylated CTD to 8% and the β-sheet increased from ∼24% to ∼36%. At ***r*** = 0.5 the α-helix further decreased down to 6% and the β-sheet increased up to ∼46%. At ***r*** = 0.7, which was approximately the saturation ratio, the CTD eventually became an all β protein, with no α-helix, ∼16% flexible regions, ∼20% turns and ∼74% β-sheet.

We also examined the secondary structure of the CTD of mouse H1e (CH1e), which shares only a 44% of sequence identity with CH1°. Like CH1°, it has three CDK sites. The unphosphorylated CH1e had a significantly higher starting proportion of α-helix (34%) and less β-structure (18%) than CH1° (Supplementary Figure 1, Table 1). Upon full phosphorylation, the amount of α-helix decreased and that

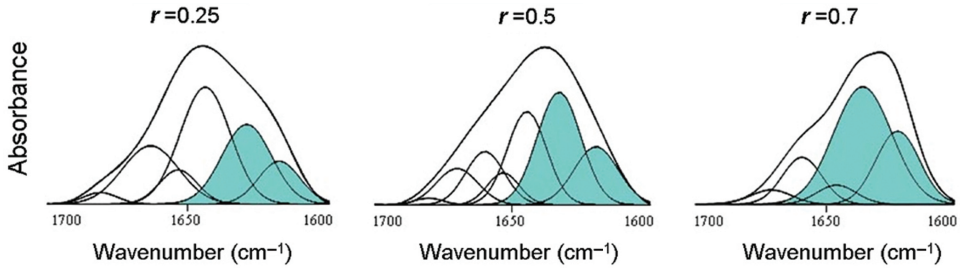

Figure 1. Amide I decomposition of DNA-bound triphosphorylated CH1° at different protein/DNA ratio (***r***) (w/w). The spectra were measured in D_2O. The buffer was 10 mM HEPES plus 140 mM NaCl, pH 7.0, at 20°C. The protein concentration was 5 mg/ml. The β-structure components are highlighted in blue.

Table 1. Percentages of secondary structure of the DNA-bound triphosphorylated (3p) CH1°

Assignment	3p										0p			
	r = 0.25				*r* = 0.5				*r* = 0.7				*r* = 0.7			
	D_2O		H_2O		D_2O		H_2O		D_2O		H_2O		D_2O		H_2O	
	Band (cm^{-1})	%	Band (cm^{-1})	%	Band (cm^{-1})	%	Band (cm^{-1})	%	Band (cm^{-1})	%	Band (cm^{-1})	%	Band (cm^{-1})	%	Band (cm^{-1})	%
Turns					1681	1							1677	6	1682	8
Turns	1681	2	1679	6	1670	10	1680	8	1671	4	1671	9	1668	13	1673	9
Turns	1663	20	1661	14	1660	13	1663	19	1659	14	1661	13	1659	15	1663	16
α-helix	1654	8			1653	6							1650	24		
α-helix/random coil			1655	21			1654	7							1652	24
Flexible regions			1641	22			1646	21			1646	6			1640	18
Random coil/ flexible regions	1644	35			1645	23			1646	6			1639	18		
Random coil[a]		13				2				0				0		
Random coil[b]				13				1				0				0
β-sheet	1630	24	1632	28	1633	31	1633	26	1636	52	1637	45	1630	16	1630	16
Low frequency β-sheet	1618	11	1616	9	1620	16	1619	19	1623	24	1624	27	1617	8	1618	9

The values corresponding to the unphosphorylated (0p) domain are included for comparison and were taken from Roque *et al.* (3).
Band position (cm^{-1}) and percentage area (%) and assignment of the components were obtained after curve fitting of the amide I band in D_2O and H_2O and in 140 mM NaCl. The values were rounded off to the nearest integer.
[a]The value corresponds to the difference between the components at 1641–46 cm^{-1} in D_2O and H_2O.
[b]The value corresponds to the difference between the components at 1650–55 cm^{-1} in H_2O and D_2O.

of β-structure increased in function of ***r***, as in CH1°, but in contrast to the latter, the fully phosphorylated CH1e conserved a significant proportion of α-helix (17%) and the increase in β-structure was less pronounced (55%).

Phosphorylation did not affect the overall conformation of the CTD free in solution. In physiological salt the conformation of both phosphorylated and unphosphorylated CTD was dominated by the random coil and turn conformations (Supplementary Table 2). Phosphorylation did not alter the proportions of secondary structure motifs in crowded conditions either (Supplementary Table 2). The specific structural changes promoted by phosphorylation appeared thus to be dependent on DNA interaction.

Site-specific effects of partial phosphorylation on the secondary structure of the DNA-bound CTD

In order to examine the effects of phosphorylation of one or two of the three TPXK sites present in CH1°, we prepared a series of single and double T→A mutants of the TPXK sites; so that, three monophosphorylated species, CH1° (p118), CH1°(p140) and CH1°(p152), and three diphosphorylated species, CH1°(p118p140), CH1°(p118p152) and CH1°(p140p152), were obtained. None of these T/A substitutions significantly altered the structure of the DNA-bound domains, as judged by the similarity of their spectra to that of the wild-type domain (Supplementary Table 3).

Of the three CDK sites, phosphorylation of T118 affected the structure the most, leading to a decrease in the α-helix content from 24% to 10% and to the appearance of 18−20% of random coil, which was absent in the unphosphorylated domain (Figure 2, Table 2). This amount of random coil together with a ∼17% of flexible regions gave a significant 35% of undefined structure. The region upstream to the first phosphorylation site is known to be in a helical conformation in the unphosphorylated domain and is thus a clear candidate for destabilization by phosphorylation at this site (21). The amount of undefined structure in CH1°(p140) was also very high (36%), but in this case the flexible regions (27%) predominated over the random coil (9%) and the α-helix decreased only slightly (down to 19%). The structure of CH1°(p152) was the closest to that of the unphosporylated domain as the changes in the proportions of secondary structure motifs did not exceed 6%. Doubly phosphorylated domains had increased amounts of random coil/flexible regions (Figure 2, Table 3). Those containing pT118, i.e. CH1°(p118p140) and CH1°(p118p152), had a low proportion of α-helix (9−10%), while in CH1°(p140p152) it decreased only slightly (17%), which also suggests that pT118 has a central role in α-helix destabilization. All mono- and diphosphorylated species had similar amounts of β-structure (∼27%), which were only slightly higher than those of the unphosphorylated domain (∼24%). The secondary structure of the mono- and diphosphorylated species was not dependent on the protein to DNA ratio (Supplementary Table 4). The dependence of the conformation on ***r*** thus appears as a specific property of the hyperphosphorylated species.

Phosphorylation had a small effect on the affinity of the CTD for the DNA

We examined the relative affinities of unphosphorylated CTD (0p), one monophosphorylated species (1p), CH1° (p118), one diphosphorylated species (2p), CH1° (p118p140) and the triphosphorylated species (3p). Relative affinities were estimated by competition of the different phosphorylated species of CH1° with an equivalent amount of the CH1t for a limited amount of DNA as previously described (Figure 3) (19). Phosphorylation caused a small decrease of the affinity of the CTD for the DNA, which was proportional to the number of phosphate groups. The apparent relative affinities were

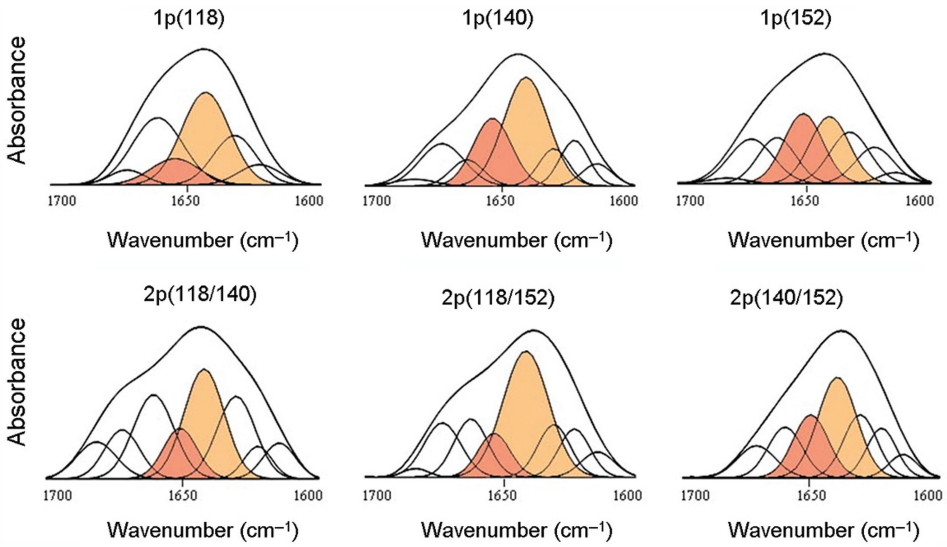

Figure 2. Amide I decomposition of the DNA-bound CH1° phosphorylated at one or two positions. The numbers in parenthesis indicate the phosphorylated position. The spectra were measured in D_2O. The buffer was 10 mM HEPES plus 140 mM NaCl, pH 7.0 at 20°C. The protein concentration was 5 mg/ml. The protein/DNA ratio (w/w) was 0.5. The α-helix component is highlighted in red and the random coil/flexible regions component is highlighted in orange.

Table 2. Percentages of secondary structure of the DNA-bound monophosphorylated species (1p) of the CH1° at $r = 0.5$

Assignment	1p(118)				1p(140)				1p(152)			
	D_2O		H_2O		D_2O		H_2O		D_2O		H_2O	
	Band (cm^{-1})	%	Band (cm^{-1})	%	Band (cm^{-1})	%	Band (cm^{-1})	%	Band (cm^{-1})	%	Band (cm^{-1})	%
Turns					1682	2	1683	2	1680	1	1681	4
Turns	1672	4	1675	16	1672	14	1674	7	1671	15	1672	7
Turns	1661	27	1665	13	1662	6	1661	11	1661	13	1660	14
α-helix	1654	10			1653	19			1650	21		
α-helix/random coil			1656	30			1655	29			1656	22
Flexible regions			1643	17			1641	27			1644	22
Random coil/flexible regions	1643	35			1640	36			1640	20		
Random coil[a]		18				9				2		
Random coil[b]				20				10				1
β-sheet	1632	17	1635	18	1630	8	1629	15	1632	16	1634	17
Low frequency β-sheet			1624	7	1622	10	1622	3	1622	11	1622	12
Low frequency β-sheet	1623	7			1614	5	1614	5	1614	3	1614	2

Band position (cm^{-1}) and percentage area (%) and assignment of the components were obtained after curve fitting of the amide I band in D_2O and H_2O and in 140 mM NaCl. The values were rounded off to the nearest integer.
The numbers in parenthesis indicate the phosphorylated positions.
[a]The value corresponds to the difference between the components at 1640–44 cm^{-1} in D_2O and H_2O.
[b]The value corresponds to the difference between the components at 1650–56 cm^{-1} in H_2O and D_2O.

Table 3. Percentages of secondary structure of the DNA-bound diphosphorylated species (2p) of the CH1° at $r = 0.5$

Assignment	2p(118/140)				2p(118/152)				2p(140/152)			
	D_2O		H_2O		D_2O		H_2O		D_2O		H_2O	
	Band (cm^{-1})	%	Band (cm^{-1})	%	Band (cm^{-1})	%	Band (cm^{-1})	%	Band (cm^{-1})	%	Band (cm^{-1})	%
Turns	1682	8	1681	3	1682	2						
Turns	1672	10	1672	6	1672	13	1680	5	1671	9	1680	8
Turns	1661	19	1660	25	1661	13	1667	18	1660	13	1668	8
α-helix	1650	10			1653	9			1650	17		
α-helix/random coil			1656	11			1656	17			1657	20
Flexible regions			1644	26			1643	31			1644	27
Random coil/flexible regions	1642	24			1641	37			1640	29		
Random coil[a]		2				6				2		
Random coil[b]				1				8				3
β-sheet	1630	18	1633	17	1630	11	1633	12	1631	16	1632	19
Low frequency β-sheet	1622	5	1621	11	1623	10	1624	10	1622	11	1622	13
Low frequency β-sheet	1615	6	1616	1	1614	5	1616	7	1615	5	1615	5

Band position (cm^{-1}) and percentage area (%) and assignment of the components were obtained after curve fitting of the amide I band in D_2O and H_2O and in 140 mM NaCl. The values were rounded off to the nearest integer.
The numbers in parenthesis indicate the phosphorylated positions.
[a]The value corresponds to the difference between the components at 1640–44 cm^{-1} in D_2O and H_2O.
[b]The value corresponds to the difference between the components at 1650–57 cm^{-1} in H_2O and D_2O.

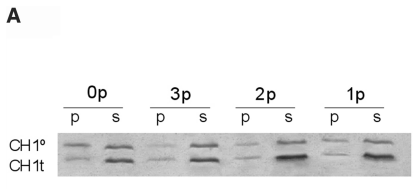

B

Apparent Relative Affinity

$k_{DNA}^{i/j}$	CH1° 0p	3p	2p	1p	(i)
CH1t	*2,56*	*0,84*	*1,85*	*2,27*	
CH1°	**1**	**0,33**	**0,72**	**0,89**	
(j)					

Figure 3. Effect of phosphorylation of CH1° on relative affinity. Competitions of pairs of CTDs for a limited amount of DNA. (**A**) The unphosphorylated CH1° (0p), the fully phosphorylated species (3p), a diphosphorylated species, CH1°/p118p144 (2p) and a monophosphorylated species, CH1°/p118 (1p), were made to compete with the unphosphorylated CH1t. p, pellet; s, supernatant. (**B**) The relative affinities of CH1° species (in bold numbers) were obtained from their relative affinities for CH1t (in italics). The values are the average of three independent determinations.

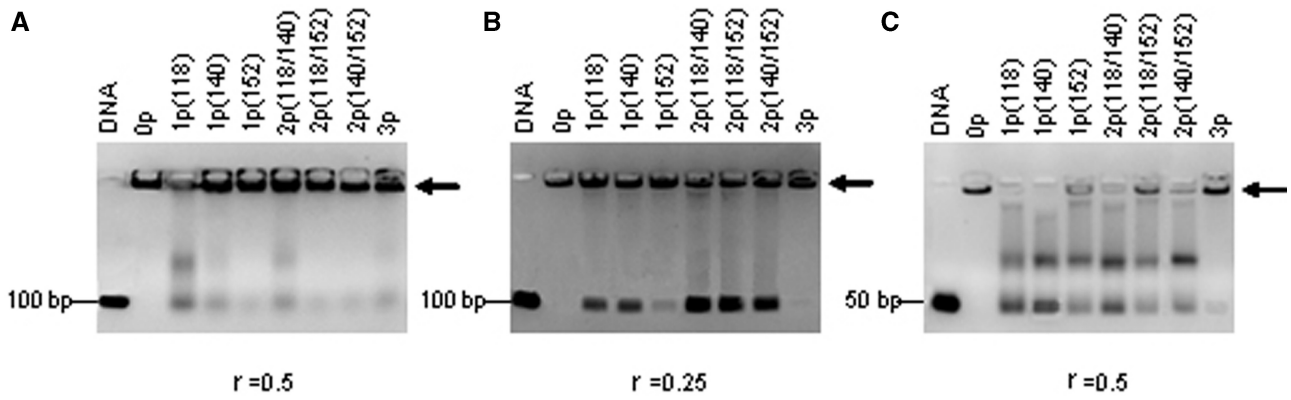

Figure 4. Electrophoretic mobility shift assay of DNA fragments with CH1° and its phosphorylated species. Binding was carried out in physiological salt (0.14 M NaCl). (**A**) DNA of 100 bp and $r = 0.5$; (**B**) DNA of 100 bp and $r = 0.25$; (**C**) DNA of 50 bp and $r = 0.5$. The arrow indicates the aggregates that do not enter the gel.

1 (0p): 0.9 (1p): 0.7 (2p): 0.3 (3p). A higher effect was not expected on a purely electrostatic basis given the small proportion of the CH1° positive charge (40 lysine residues) represented by the incorporated phosphate groups (a maximum of three). In contrast, sea-urchin testis-specific H1 and H2B have most basic amino acids residues in their N-terminal regions in multiple SPKK sites; in this case, general Ser phosphorylation could effectively abolish the net charge of the entire N-terminal region and thus greatly weaken its interaction with DNA (22).

Differential aggregation of DNA fragments by fully and partially phosphorylated CTD

The capacity of unphosphorylated CTD and its different phosphorylated species to aggregate DNA fragments was investigated by band-shift-gel-electrophoresis. With DNA fragments of 100 bp and $r = 0.5$, the unphosphorylated CTD and all phosphorylated species formed large complexes that could not enter the gel (Figure 4A). Decreasing either the size of the DNA or the r value revealed different aggregation capacities for the different CTD forms. Figure 4B and C shows bandshift assays with DNA fragments of 100 bp at $r = 0.25$ and with DNA fragments of 50 bp at $r = 0.5$. In both conditions, the unphosphorylated C-terminus aggregated the totality of the DNA fragments. Phosphorylation of either one or two sites decreased the aggregation capacity of the C-terminus significantly. Surprisingly, the hyperphosphorylated C-terminus regained to a large extent the aggregation capacity of the unphosphorylated C-terminus, displaying a strong aggregation band and little free DNA.

Electron microscopy of the DNA complexes confirmed the bandshift results. The complexes had varied morphologies, but the aggregates formed with either unphosphorylated or fully phosphorylated CTD were consistently larger and denser than those with partially phosphorylated species (Supplementary Figure 2).

DISCUSSION

We have shown that full phosphorylation of the DNA-bound CTD brings about a large structural change consisting in a significant increase in β-structure accompanied by a decrease in α-helix. The effect is apparent at the lowest r values ($r = 0.15$), but is favored by the saturation of the DNA lattice, suggesting that protein-protein interactions contribute to the conformational transition. Partial phosphorylation induces in general a large proportion of undefined structure (random coil and flexible regions), but, in contrast to full phosphorylation, it does not lead to a significant increase in β-structure.

The increase of β-sheet content and the loss of α-helical structure in the H1 CTD following full phosphorylation is a kind of structural conversion similar to that observed in amyloidogenic proteins during fibril formation (23). In prion encephalopaties, the analogy can be pushed further as it has been shown that interaction with DNA converts the α-helical cellular isoform into a β-isoform similar to that found in the fibrilar state (24). Furthermore, H1 has been found associated to amyloid-like fibrils (25).

The effects of phosphorylation on the affinity of the CTD for the DNA were moderate: a three-fold decrease for the fully phosphorylated domain and smaller effects for the mono- and diphosphorylated species. It is interesting to note that in spite of its lower affinity for DNA, the fully phosphorylated domain showed a higher aggregation capacity of DNA fragments than the partially phosphorylated species. The aggregation capacity of the fully phosphorylated species was indeed nearly as high as that of the unphosphorylated domain. The high condensing capacity of the fully phosphorylated species might have a structural basis. A general feature of the sequences of the CTD of H1 histones is the large proportion of basic residues present as doublets: about 75% in mammalian somatic subtypes. In β-sheets, consecutive side chains project alternatively above and below the sheet-like structure. It is likely that the abundance of Lys doublets together with the β-sheet structure generates a binding motif with two cationic surfaces, particularly in the hyperphosphorylated CTD. Such a structure seems well suited to the electrostatic crosslinking of two segments of DNA.

The site-specificity of the effects of phosphorylation on the secondary structure and DNA condensing capacity of the CTD, together with the moderate effect of

phosphorylation on the affinity for the DNA, suggest that the effects of phosphorylation are mediated by specific structural changes and are not a simple effect of the net charge. According to this, the properties of hyperphosphorylated H1 would not represent the extreme of a continuous variation in molecular properties depending on the number of phosphates, but would be determined by the specific structures associated with full phosphorylation.

The reasons for general H1 hyperphosphorylation in metaphase chromosomes remain unclear. However, the specific structural features, in particular the high β-sheet content and the higher aggregation capacity of the fully phosphorylated domain suggest that hyperphosphorylation may play a role, together with other condensing factors, in metaphase chromatin condensation. Conversely, the loss of defined structure and the lower condensing capacity of some mono- and diphosphorylated species could explain the relaxing effect of partially phosphorylated H1 on chromatin structure during interphase, particularly in S phase.

Some reports support the occurrence of opposite effects of moderate as opposed to full phosphorylation. SV40 minichromosomes reconstituted with either unphosphorylated or hyperphosphorylated H1 were more compact and less efficient as substrate in *in vitro* replication compared with minichromosomes reconstituted with moderately phosphorylated H1 (26). It has been suggested that hyperphosphorylation of histone H1 and H3 leads to inhibition of glucocorticoid receptor-mediated chromatin remodeling and inactivation of the mouse mammary tumor virus (MMTV) promoter by preventing the association of transcription factors with the promoter *in vivo*. In contrast, a moderate amount of H1 phosphorylation contributes significantly to the induction of transcription from the MMTV promoter (27). It has also been shown that phosphorylation of only one site within the CTD of H1b severely disrupts the interaction between H1b and the heterochromatin protein 1α (HP1α), a key component of mammalian heterochromatin (28).

Chromatin condensation associated with hyperphosphorylation in metaphase chromosomes may be structurally and mechanistically distinct from other condensed chromatin states associated with unphosphorylated H1, such as those of chicken erythrocyte nuclei (29), sea urchin sperm (30), *Tetrahymena* macronuclei or interphase heterochromatin (31). Figure 5 shows a schematic representation of some H1 related factors that may be involved in the transition between relaxed and condensed chromatin in different systems.

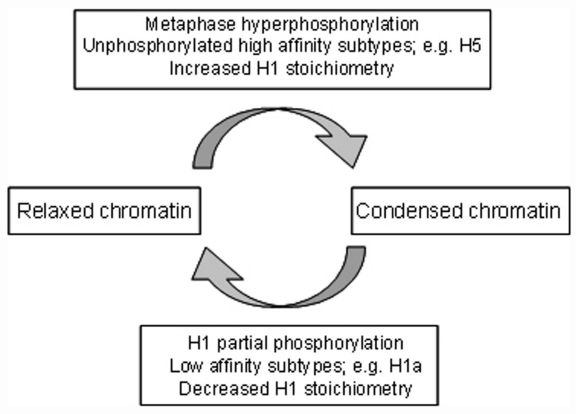

Figure 5. H1 related factors involved in the transition between relaxed and condensed chromatin.

SUPPLEMENTARY DATA

Supplementary Data are available at NAR Online.

ACKNOWLEDGEMENTS

We thank O. Castell for his help with the electron microscopy experiments. Ministerio de Educación y Ciencia (Spain), Grant BFU2005-02143. Funding to pay the Open Access publication charges for the article was provided by Grant BFU2005-02143.

Conflict of interest statement. None declared.

REFERENCES

1. Zlatanova,J., Caiafa,P. and van Holde,K. (2000) Linker histone binding and displacement: versatile mechanism for transcripcional regulation. *FASEB J.*, **14**, 1697–1704.
2. Hartman,P.G., Chapman,G.E., Moss,T. and Bradbury,E.M. (1977) Studies on the role and mode of operation of the very-lysine-rich histone H1 in eukaryote chromatin. The three structural regions of the histone H1 molecule. *Eur. J. Biochem.*, **77**, 45–51.
3. Lu,X. and Hansen,J.C. (2003) Revisiting the structure and functions of the linker histone C-terminal tail domain. *Biochem. Cell Biol.*, **81**, 173–176.
4. Roque,A., Iloro,I., Ponte,I., Arrondo,J.L. and Suau,P. (2005) DNA-induced secondary structure of the carboxyl-terminal domain of histone H1. *J. Biol. Chem.*, **280**, 32141–32147.
5. Gunasekaran,K., Tsai,C.J., Kumar,S., Zanuy,D. and Nussinov,R. (2003) Extended disordered proteins: targeting function with less scaffold. *Trends Biochem. Sci.*, **28**, 81–85.
6. Bracken,C., Iakoucheva,L.M., Romero,P.R. and Dunker,A.K. (2004) Combining prediction, computation and experiment for the characterization of protein disorder. *Curr. Opin. Struct. Biol.*, **14**, 570–576.
7. Dyson,H.J. and Wright,P.E. (2005) Intrinsically unstructered proteins and their functions. *Nat. Rev. Mol. Cell Biol.*, **6**, 197–208.
8. Roque,A., Ponte,I. and Suau,P. (2007) Macromolecular crowding induces a molten globule state in the C-terminal domain of histone H1. *Biophys. J.*, **93**, 2170–2177.
9. Swank,R.A., Th'ng,J.P., Guo,X.W., Valdez,J., Bradbury,E.M. and Gurley,L.R. (1997) Four distinct cyclin-dependent kinases phosphorylate histone H1 at all of its growth-related phosphorylation sites. *Biochemistry*, **36**, 13761–13768.
10. Talasz,H., Helliger,W., Puschendorf,B. and Lindner,H. (1996) In vivo phosphorylation of histone H1 variants during the cell cycle. *Biochemistry*, **35**, 1761–1767.
11. Bradbury,E.M., Inglis,R.J., Matthews,H.R. and Sarner,N. (1973) Phosphorylation of very-lysine-rich histone in Physarum polycephalum. Correlation with chromosome condensation. *Eur. J. Biochem.*, **33**, 131–139.
12. Sarg,B., Helliger,W., Talasz,H., Förg,B. and Lindner,H.H. (2006) Histone H1 phosphorylation occurs site-specifically during interphase and mitosis: identification of a novel phosphorylation site on histone H1. *J. Biol. Chem.*, **281**, 6573–6580.
13. Roth,S.Y. and Allis,C.D. (1992) Chromatin condensation: does histone H1 dephosphorylation play a role? *Trends Biochem. Sci.*, **17**, 93–98.
14. Contreras,A., Hale,T.K., Stenoien,D.L., Rosen,J.M., Mancini,M.A. and Herrera,R.E. (2003) The dynamic mobility of histone H1 is

regulated by cyclin/CDK phosphorylation. *Mol. Cell Biol.*, **23**, 8626–8636.
15. Lever,M.A., Th'ng,J.P.H., Sun,X. and Hendzel,M. (2000) Rapid Exchange of histone H1.1 on chromatin in living cells. *Nature*, **408**, 873–876.
16. Th'ng,J.P., Guo,X.W., Swank,R.A., Crissman,H.A. and Bradbury,E.M. (1994) Inhibition of histone phosphorylation by staurosporine leads to chromosome decondensation. *J. Biol. Chem.*, **269**, 9568–9573.
17. Arrondo,J.L. and Goñi,F.M. (1999) Structure and dynamics of membrane proteins as studied by infrared spectroscopy. *Prog. Biophys. Mol. Biol.*, **72**, 367–405.
18. Vila,R., Ponte,I., Collado,M., Arrondo,J.L. and Suau,P. (2001) Induction of secondary structure in a COOH-terminal peptide of histone H1 by interaction with the DNA: an infrared spectroscopy study. *J. Biol. Chem.*, **276**, 30898–30903.
19. Orrego,M., Ponte,I., Roque,A., Buschati,N., Mora,X. and Suau,P. (2007) Differential affinity of mammalian histone H1 somatic subtypes for DNA and chromatin. *BMC Biol.*, **5**, 22.
20. Rickwood,D. and Hames,B.D. (1990) Gel electrophoresis of Nucleic Acids a Practical Approach, IRL Press, Oxford.
21. Vila,R., Ponte,I., Jiménez,M.A., Rico,M. and Suau,P. (2000) A helix-turn motif in the C-terminal domain of histone H1. *Protein Sci.*, **9**, 627–636.
22. Green,G.R., Lee,H.J. and Poccia,D.L. (1993) Phosphorylation weakens DNA binding by peptides containing multiple "SPKK" sequences. *J. Biol. Chem.*, **268**, 11247–11255.
23. Aguzzi,A. and Polymenidou,M. (2004) Mammalian prion biology: one century of evolving concepts. *Cell*, **116**, 313–327.
24. Cordeiro,Y., Machado,F., Juliano,L., Juliano,M.A., Brentani,R.R., Foguel,D. and Silva,J.L. (2001) DNA converts cellular prion protein into the β-sheet conformation and inhibits prion peptide aggregation. *J. Biol. Chem.*, **276**, 49400–49409.
25. Duce,J.A., Smith,D.P., Blake,R.E., Crouch,P.J., Li,Q.X., Masters,C.L. and Trounce,I.A. (2006) Linker histone H1 binds to disease associated amyloid-like fibrils. *J. Mol. Biol.*, **361**, 493–505.
26. Halmer,L. and Gruss,C. (1996) Effects of cell cycle dependent histone H1 phosphorylation on chromatin structure and chromatin replication. *Nucleic Acids Res.*, **24**, 1420–1427.
27. Bhattacharjee,R.N. and Archer,T.K. (2006) Transcriptional silencing of the mouse mammary tumor virus promoter through chromatin remodelling is concomitant with histone H1 phosphorylation and histone H3 hyperphosphorylation at M phase. *Virology*, **346**, 1–6.
28. Hale,T.K., Contreras,A., Morrison,A.J. and Herrera,R.E. (2006) Phosphorylation of the linker histone H1 by CDK regulates its binding to HP1alpha. *Mol. Cell*, **22**, 693–699.
29. Wagner,T.E., Hartford,J.B., Serra,M., Vandegrift,V. and Sung,M.T. (1977) Phosphorylation and dephosphorylation of histone V (H5): controlled condensation of avian erythrocyte chromatin. Phosphorylation and dephosphorylation of histone H5. II. Circular dichroic studies. *Biochemistry*, **16**, 286–290.
30. Poccia,D. (1989) *The molecular biology of fertilization*. In Schatten,H. and Schatten,G. (eds), Academic Press, New York, pp. 115–135.
31. Roth,S.Y., Schulman,I.G., Richman,R., Cook,R.G. and Allis,C.D. (1988) Characterization of phosphorylation sites in histone H1 in the amitotic macronucleus of Tetrahymena during different physiological states. *J. Cell Biol.*, **107**, 2473–2482.